Chapter 7
Photonic Crystals as Robust Label-Free Biosensors

Mark A. Lifson and Benjamin L. Miller

Abstract This chapter focuses on a highly sensitive class of label-free optical sensor: photonic crystals (PhCs). One- and two-dimensional versions of these structures (1D-PhC, 2D-PhC) can be readily fabricated using standard techniques from the microelectronics industry. While many research groups have contributed to development of PhCs in the context of biosensing, the chapter primarily focuses on efforts from several groups at the University of Rochester. We discuss novel photonic crystal designs, methods to capture and quantify small molecules, proteins, and viruses with photonic crystals, and remarkable approaches to improving photonic crystals in terms of their ultimate limit of detection and sensitivity. Looking forward, we also discuss new ways to use photonic crystals to discriminate between specific and non-specific binding.

7.1 Introduction

Biosensor technology has evolved rapidly over the last five decades. One of the first biosensors was an electrochemical sensor that, in the presence of glucose, determined oxygen concentration using the enzyme glucose oxidase [1]. For the detection of large and complex molecules (such as bacteria, protein, and viruses), it was necessary to produce schemes for amplifying signals produced by target binding, due to the lack of sensitive biosensing transducers. One of the earliest methods used to amplify biological signals was the incorporation of radioactive nuclides, which were read out using a Geiger counter to determine concentrations [2–4]. As technology improved,

M. A. Lifson · B. L. Miller (✉)
Department of Biomedical Engineering, University of Rochester,
Rochester, NY 14642, USA
e-mail: Benjamin_miller@urmc.rochester.edu

M. A. Lifson · B. L. Miller
Department of Dermatology, University of Rochester, Rochester, NY 14642, USA

M. J. Serpe et al. (eds.), *Photonic Materials for Sensing, Biosensing and Display Devices*, Springer Series in Materials Science 229,
DOI 10.1007/978-3-319-24990-2_7

alternatives were developed such as enzyme-substrate amplification (horseradish peroxidase [5], alkaline phosphatase [6, 7]), and chemically linked fluorescent labels [8]. Though these methods remain popular and widely used, there has been a recognition in both the academic and commercial sectors that devices which can directly measure biological material are desirable both from the workflow improvements they can provide, but also because the use of labels and secondary reagents can hinder the versatility and accuracy of the assay [9, 10]. One class of "label-free" sensors centers on monitoring changes in the optical properties of substrates with bound material on their surfaces, including light polarization (ellipsometery), light intensity (thin film interferometers), or refractive index (surface plasmon resonance) [11–13]. Generally, these devices follow the same modular format in which receptor (probe) molecules are first immobilized onto a substrate, and then immersed in a solution to identify the presence of its partner ligand (analyte). More recently, advances in nanofabrication have enabled the development of substrates that guide and interact with light *inside* of their volume, such as waveguides, spectral gratings, optical reflectors, and optical absorbers [14, 15]. Due to their small size, these devices require very few receptor/ligand interactions to produce a signal due to the enhanced material interaction inside the substrate volume, resulting in increased device sensitivity [16]. Devices such as toroidal and ring resonators, optical cavities, interferometers, and waveguides have been used to sense biological materials including proteins, bacteria and viruses [17–19]. While still at a relatively early stage, both interferometric methods and ring resonators have been commercialized.

This chapter focuses primarily on one particularly attractive label-free sensor: the two-dimensional photonic crystal (2D-PhC). Due to its remarkable sensitivity, small footprint, and low cost, photonic crystals were initially investigated for telecommunications applications, but subsequently became of interest as transducers in a wide variety of label-free biosensing applications. The working principles of the 2D-PhC are based on the underlying structure of the substrate, which is engineered to contain a periodic variation in the dielectric constant in two spatial directions (e.g., a series of wells arranged in a hexagonal pattern on a substrate; a simpler photonic crystal design, which we also discuss, is called a 1-D PhC and only varies periodically in one dimension). Such devices exhibit a tunable photonic bandgap (PBG), which selectively allows (or blocks) a range of light wavelengths. Often, the periodic translational symmetry of the PhC is interrupted with a defect, creating a localized mode within the PBG [20]. For example, when a row of pillars or wells is removed from the lattice, light can be guided around tight corners (90°), which is an impossible task with fiber-based waveguides [21]. High Q-factor resonators (where "Q", the "quality factor" of the device, is defined by the ratio of the resonance frequency and its full width at half-maximum bandwidth) can be formed by introducing a defects into a 1- or 2D lattice to change the shape and confinement of the electric field. Since the electric field is strongly confined near the defects, changes in the local refractive index will result in a shift in the position of the localized mode. Using a tunable laser, it is possible to measure the optical changes occurring within a 2D-PhC by monitoring positions of this resonance. The initial

position of the peak is used as a baseline, and subsequent incubation with biological material will shift the position of the peak due to the refractive index changes occurring in the crystal (and particularly within and close to the defect) upon binding. The degree of peak shifting corresponds directly to the amount of material present. In this way, 2D-PhCs detect the presence of biological material by monitoring the shifts in absorption dips, and can quantify the concentration of chemical or biological targets in a sample [22].

While this chapter focuses primarily on the current state of the art in 2D-PhC based biosensing, it is useful to first discuss earlier efforts to develop sensors based on a simpler structure, the 1D PhC. Here, as in the remainder of the chapter, we will primarily focus on efforts by several groups at the University of Rochester, rather than being comprehensive. Many groups world wide have also made critical contributions to our understanding of the design principles and capabilities of PhC sensors.

7.2 1D-PhCs in Biosensing

Most of the early research into the use of 1-D PhCs as chemical and biosensors centered on a material called porous silicon. Originally discovered in the 1950s independently by Ulhir [23] and Turner [24], research into the uses of porous silicon accelerated when its room temperature photoluminescence was first observed by Canham and colleagues [25]. Porous silicon is produced when n- or p-type silicon is subjected to an electrochemical etch in hydrofluoric acid. By varying the etchant composition (HF alone, or HF plus a cosolvent) porous silicon may be produced with a wide range of pore sizes. These materials are generally described as members of one of three groups: nanoporous silicon (pore size <10 nm), mesoporous silicon (10–100 nm) or macroporous silicon (100 nm and higher). Porous silicon has an inherent optical response, either viewed in reflection or, for some types, as luminescence due to nanocrystalline silicon particles remaining within the pores. Of relevance to our discussion here, the density of pores produced during the etching process may be changed as a function of current density. Changes in the porosity of porous silicon produce differences in the refractive index of the material, which in turn are visible as differences in the optical properties (Fig. 7.1a). Since etching only occurs at an appreciable rate at the interface between the etchant solution and unmodified silicon, this means that the pore density (or, porosity) of the silicon, and hence the refractive index of the material, may be changed in a precise and programmable way. This allows for the production of complex structures including Bragg mirrors or microcavities, both examples of 1-D PhCs. An example of a porous silicon microcavity is shown in Fig. 7.1b. Early work on the use of porous silicon in optical sensing was conducted in parallel by the Rochester team and by the Sailor and Ghadiri groups [26, 27]; here, we will focus on applications using 1-D PhCs.

The first example of a 1-D porous silicon PhC microcavity biosensor involved a device derivatized with a 30 base-pair DNA probe specific for lambda

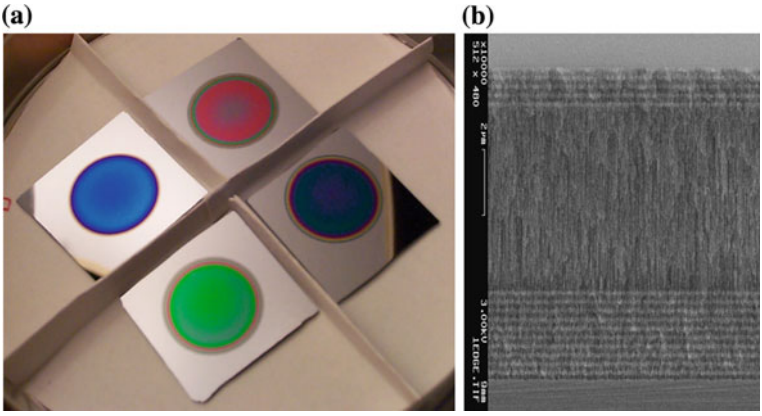

Fig. 7.1 **a** Porous silicon sensors. Each chip has a different pore density, producing readily observable differences in the reflectance spectrum. **b** Scanning electron micrograph of a microcavity resonator, or 1-D PhC, fabricated in porous silicon. Two multilayer mirrors flank an "active", or defect layer

bacteriophage. When treated with genomic DNA from lambda bacteriophage, the sensor yielded a strong red shift in its luminescence spectrum. In a control experiment, no red shift was observed for a sensor treated with synthetic, mismatched DNA [28]. While encouraging, questions remaining after this initial result included whether a porous silicon 1-D PhC sensor could be employed using other types of molecules as capture agents, and whether such a device could selectively detect a target in a complex biological sample. To address this question, a porous silicon microcavity sensor was functionalized with TWTCP (Fig. 7.2a), a designed, synthetic receptor for bacterial lipid A [29]. Since lipid A is a characteristic cell membrane constituent of Gram-(−) bacteria, it was anticipated that this sensor would constitute a silicon analog of the venerable Gram stain (in which a dye specifically adheres to lipoteichoic acid, a major constituent of Gram-(+) bacteria). Indeed, treatment of the sensor with lysate from *Escherichia coli*, a Gram-(−) bacterium, produced a readily discernible red shift (Fig. 7.2b) [30]. In contrast, exposure of the sensor to lysate from *Bacillus subtilis*, a common Gram-(+) soil bacterium, produced no change in the luminescence spectrum.

Macroporous 1D PhC structures are also suitable for biosensing, as detailed in a 2005 report of antibody-antigen detection [31]. While porosity of 1D PhCs may be tuned in order to favor infiltration of specific target analytes, an important feature of porous silicon is that its structure inherently prevents infiltration by large constituents of a sample. This is potentially useful in the context of diagnostics, as demonstrated most convincingly by an SEM image from the work of DeLouise and colleagues showing a red blood cell unable to penetrate a porous silicon matrix (Fig. 7.3). The DeLouise group has also provided a rare direct comparison between

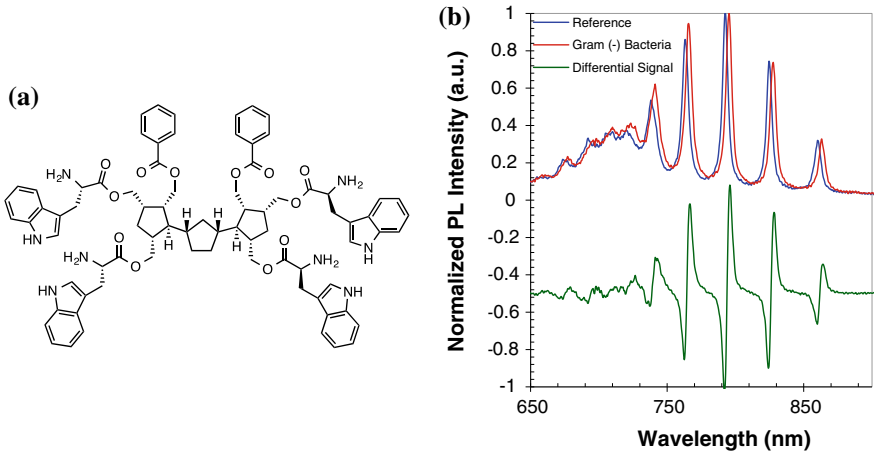

Fig. 7.2 **a** TWTCP, a synthetic receptor for bacterial lipid A. Treatment of a TWTCP-functionalized porous silicon 1D PhC with Gram-(−) bacterial lysate produces a red shift due to lipid A binding (**b**), while no signal is observed following exposure to a Gram-(+) bacterium

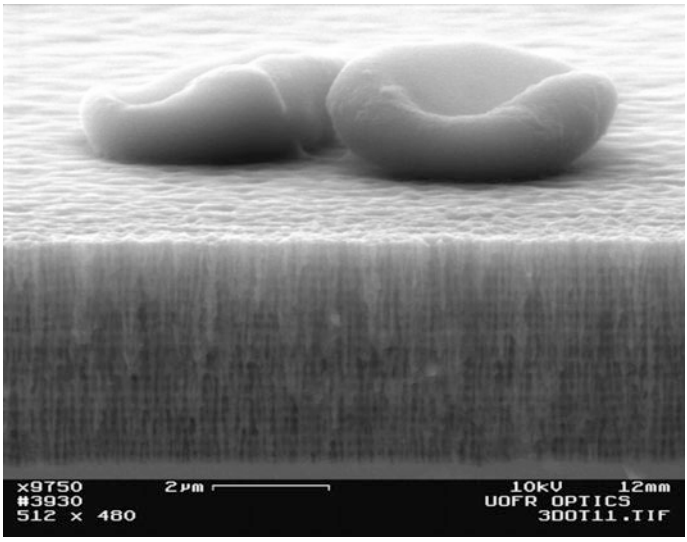

Fig. 7.3 SEM image highlighting the ability of porous silicon (here, a Bragg mirror of mesoporous silicon) to prevent infiltration of large sample constituents, such as a red blood cell (*courtesy* Dr. Lisa Bonanno and Prof. Lisa DeLouise)

the performance of a PhC sensor and a commercial diagnostic assay, in the context of developing an optical sensor for morphine. Here, a competitive assay for morphine and morphine derivatives was developed, and was found to provide results equivalent to those provided by the clinical assay [32].

While most experiments with porous silicon sensors have focused on materials embedded in a solid silicon wafer, it is possible for these devices to function following removal from the underlying substrate (which can be effected by a strong, electropolishing current at the end of the etch process). In a particularly notable example of this, the Rochester group reported in 2005 that a porous silicon sensor could be embedded in a hydrogel bandage material, and that its optical response was essentially unchanged after repeated cycles of hydration and drying over the course of a full year [33].

In addition to 1D PhCs fabricated in porous silicon, other materials systems have been the subject of considerable research and, in one case, even commercialization. The Cunningham group in particular has demonstrated a series of applications for 1D photonic crystal polymers; [34–36] these can be manufactured at large scale, and have been integrated with 96- and 384-well microtiter plates. A closely related technology has been commercialized by Corning, Inc. as the Epic® system. In a very different design, evanescently coupled 1-D PhCs have been fabricated by Erickson and colleagues. When coupled with optofluidic (i.e. optical forces combined with microfluidic forces) manipulation of analytes, these sensors have demonstrated very high sensitivity for targets [37].

7.3 Design, Development, and Optimization of 2D-PhCs

While our group and many others have (as discussed above) produced notable successes in the use of 1D PhCs for sensing, the potential for dramatically reducing the interaction volume, and in turn driving a dramatic increase in sensitivity, led to research on 2D PhCs. Several 2D-PhC designs have been examined in the context of biological and chemical sensing. In particular, our work has centered on the use of structures in which a single defect provides a readily observable resonance peak to detect the binding of target analyte, and as such will be the main focus of the remainder of this chapter [22, 38–40].

Our initial photonic crystal design included input and output waveguides terminating at the array, and a point defect (a hole with a larger diameter) in the center of the crystal (Fig. 7.4a). The optical spectrum for these devices have photonic bandgaps formed through the destructive interference of incident light, with the exception of a single wavelength which was transmitted through the crystal as a result of the perturbation in periodicity from a large point defect. A different design was also pursued, where a waveguide passing through a hexagonal array of air holes allowed many optical modes to be guided through the crystal within the photonic bandgap, with the exception of a single wavelength, which was absorbed as a result of the perturbation in periodicity from a smaller point defect (Fig. 7.4b).

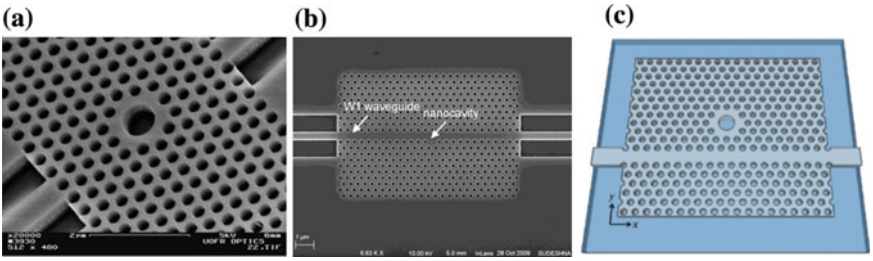

Fig. 7.4 SEM images of two dimensional photonic crystals with three different designs. **a** A large defect (600 nm) within a triangular lattice of smaller diameter (235 nm) air wells on a silicon-on-insulator wafer [39], **b** A small diameter defect (110 nm) within a triangular lattice of smaller diameter (235 nm) air wells and a removed row of wells (w1 waveguide) [38], and **c** A proposed design with a large diameter defect and a removed row of wells (w1 waveguide) [41]

This design allowed for multiplexing of many crystals along a single waveguide, since almost all optical modes, except those absorbed by the point defects, passed through the crystals. Our most recent design included a point detect that was larger than the surrounding lattice, and also included a w1 waveguide (i.e. a waveguide having the width of a single row) (Fig. 7.4c). Because the electric field is strongly localized to the defect region, having a well that was larger than the surrounding lattice could provide a means to selectively capture large biotargets such as viruses.

Typically, 2D-PhCs are fabricated using top-down approaches in a clean-room environment. The feature sizes of 2D-PhCs are accessible via widely used commercial photolithographic techniques. However, because research has focused on devices still in the prototyping stage, fabrication processes are typically performed using electron-beam lithography, since creating new masks with each design change is cost prohibitive when using photolithography. For all aforementioned designs, two different processes were used for 2D-PhC fabrication and were developed using a silicon-on-insulator wafer, which is comprised of a silicon layer (400 nm), buried oxide layer (1000 nm), and a silicon slab (>1 mm). The first process uses a negative electron-beam resist, polymethyl methacrylate (PMMA), to create features in SOI (Fig. 7.5top), while the second process uses a positive resist, hydrogen silsesquioxane (HSQ), (Fig. 7.5bottom).

Negative Resist:

1. Figure 7.5a, top: Oxide is first grown on an SOI wafer using a tube furnace, where ~100 nm of the underlying silicon layer is used to create ~150 nm of oxide. The process takes approximately 8 h.
2. Figure 7.5b, top: A negative resist is spun onto the wafer and cured for ~1 h.
3. Figure 7.5c, top: Locations to be removed (negative) are exposed to an electron beam to weaken the resist. This process takes on average 8 h, although the total time is dependent on the number of structures to be fabricated.
4. Figure 7.5d, top: The weakened resist is developed and washed away, leaving behind areas masked by unexposed resist.

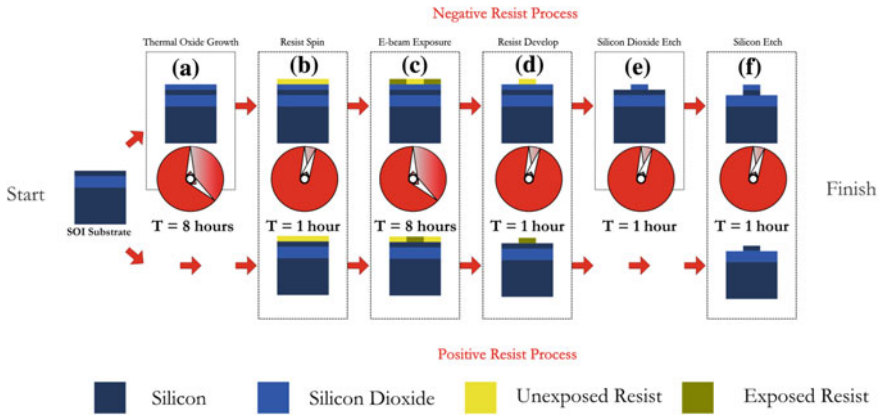

Fig. 7.5 Fabrication process for 2D-PhCs using a negative resist (*top*) or a positive resist (*bottom*). Steps include oxide growth (**a**), resist (**b**), electron-beaming (**c**), developing (**d**), silicon dioxide etching (**e**), and silicon etching (**f**)

5. Figure 7.5e, top: The resist is used as a soft mask for the underlying silicon oxide layer during a silicon dioxide-specific etch process.
6. Figure 7.5f, top: The leftover silicon oxide is then used as a hard mask for the underlying device layer (silicon), during a silicon-specific etch process.

Positive Resist:

1. Figure 7.5b, bottom: A positive resist is spun onto the wafer, no curing necessary.
2. Figure 7.5c, bottom: Locations to be masked (positive) are exposed to an electron beam to harden the resist. This process takes approximately 8 h, although the total time is dependent on the number of structures to be fabricated.
3. Figure 7.5d, top: The unhardened resist is developed and washed away, leaving behind areas masked by exposed resist.
4. Figure 7.5f, top: The resist is used as a soft mask for the underlying silicon layer during a silicon-specific etch process.

7.4 Biosensing with 2D-PhCs

While many different designs for 2D-PhCs have been proposed over the last decade, the Rochester group has been at the forefront of using them for the detection of biologically relevant targets. In the first report, a small defect design was used to measure transmission of light through the crystal after functionalization with capture molecules (Fig. 7.6a). The crystal was first modified with an amino silane followed by gluteraldehyde, allowing covalent capture of proteins and peptides via

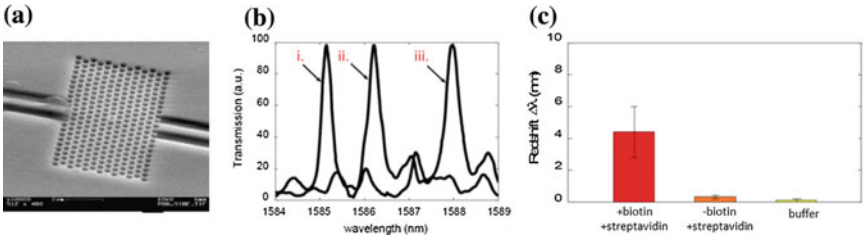

Fig. 7.6 Initial photonic crystal design (**a**), where spectrum measurements after silanization and oxidation (**b** i.), followed by gluteraldehyde (**b** ii.) and bovine serum albumin (**b** iii.) caused significant red-shifting of the maximum wavelength. Specificity and selectivity were determined using the same functionalization procedure for biotin binding streptavidin. Results demonstrated for the first time that 2D-PhCs could be used to detect biological molecules

reaction with surface lysines. After oxidation and silanization (Fig. 7.6b i.), gluteraldehyde treatment (Fig. 7.6b ii.), and bovine serum albumin deposition (Fig. 7.6b iii.) a spectrum was collected, and the red-shift of the defect resonance was observed. This non-specific, covalent capture of bovine serum albumin conclusively showed that proteins could be captured within the crystal surface and observed by measuring red-shifts. Specific detection was also measured using gluteraldehyde-immobilized biotin to capture streptavidin; significantly more streptavidin binding was observed relative to a chip lacking biotin Fig. 7.6c). Results with this design suggested that the limit of detection was approximately 2.5 fg, assuming a monolayer of material. This work set the stage for using 2D-PhCs to detect biological targets, and described a robust silane and gluteraldehyde surface chemistry for direct and covalent immobilization of proteins to the transducer surface, proving that the small sub-micron wells could be readily functionalized with biomolecules [22].

While this initial work studied the red-shift in response to non-specific binding, and high binding affinity pairs ($K_D \approx 10^{-15}$ mol/L), the response of the device for antibody/antigen interactions with more typical association thermodynamics was unknown. To answer this question, a different crystal design was used to measure lower affinity ($K_D \approx 10^{-9}$ mol/L) antibody/antigen interactions [42]. With this new design, crystals with slightly different defects were connected with a w1 waveguide to allow transmission of almost all wavelengths of light, except for those that were strongly absorbed independently by each crystal (Fig. 7.7a). Multiplexed devices were used to simultaneously measure multiple maximum wavelengths using a single waveguide and only one wavelength scan, providing redundant and statistically relevant data without having to run a separate control (Fig. 7.7b).

Since this design was robust and compact, large-scale protein binding studies could be performed. A dose-response experiment using multiplexed crystals functionalized with anti-human immunoglobulin gamma (IgG) specifically captured human IgG with a detection limit in the low nanomolar range (Fig. 7.7c) [38]. The calculated K_D for the h-IgG/IgG interaction based on these experiments was 7.2×10^{-7} mol/L, in agreement with values previously reported in the literature.

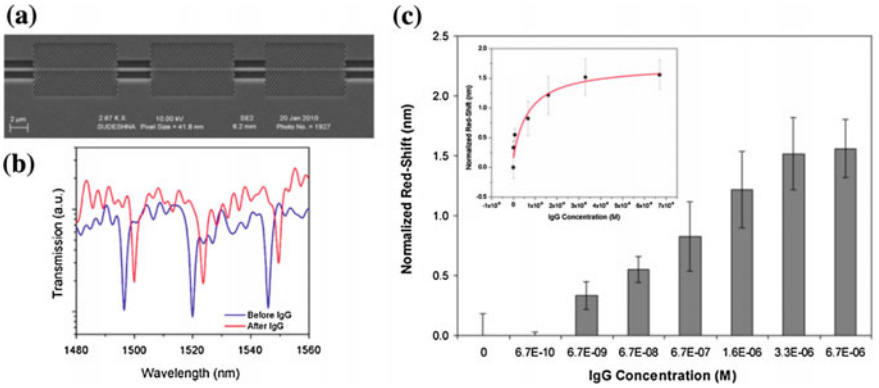

Fig. 7.7 Multiplexable, error-corrected 2D-PhC design (**a**). Multiple in-series crystals, with slightly different defect sizes, connected with waveguides could be used to track multiple red-shifts simultaneously on a single spectrum (**b**). Using this design, a dose-response for human immunoglobulin gamma (h-IgG) capture using anti-human IgG was experimentally determined (**c**). Error bars represent standard deviations from multiple measurements (n = 5)

These results indicated that the binding thermodynamics and biological interactions were well preserved and detectable with 2D-PhCs. Furthermore, this preliminary work suggested that 2D photonic crystals could be sufficient for real-time affinity analysis of biological molecules, if appropriate microfluidics were incorporated, since it was found to be sensitive to biomolecular capture in the relevant concentration ranges for these types of analyses.

Although label-free protein detection is important, there is a significant need to detect low levels of viruses that are known to be harmful to humans (e.g. human immunodeficiency virus, hepatitis B, human papillomavirus, etc.). Typical screening assays identify secondary reports to the virus (such as antibodies), which are detected many weeks after patients seroconvert from an acute infection. Therefore, it is important that viruses are measured directly and at the lowest possible concentration since a significant proportion of new infections, such as with HIV, are from individuals that have recently been infected [43]. While gold-standard nucleic acid-based tests can match the theoretical sensitivities of ultra-sensitive devices (detection can be performed down to single copies), the process is subject to large uncertainties and biases while also being labor intensive and time consuming to perform, since complex sample preparation steps are required [44–46]. Motivated by these reasons, researchers have attempted to use optical technologies for detection of whole viruses, since they strongly interact with light due to their large refractive index change per unit area [47, 48]. One attractive aspect of the 2D-PhC structures developed by the Rochester group is that the configuration of the substrate is particularly well suited for whole virus detection, since simulations show that the device is highly sensitive to materials which are size matched to the to the sensing regions, such as virus particle diameters (Fig. 7.8). Although the defect region is the most sensitive (largest light/matter interaction),

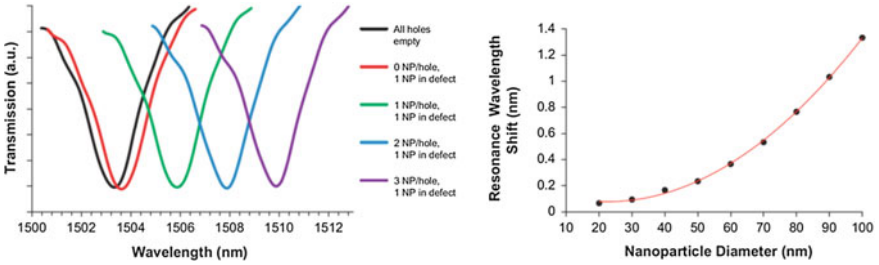

Fig. 7.8 Simulated transmission spectra of a 2D-PhC interacting with different numbers of nanoparticles inside the defect, neighboring wells, or combination (*left*). Simulated red-shift of a 2D-PhC design in response to differently sized nanoparticles infiltrating the defect (*right*). Results show that there is an observable red-shift for virus-sized objects

the surrounding wells can also interact with the electric field, albeit to lesser degrees, but still contribute a substantial amount of red-shift when material is bound to all of their interiors, such as capture of many virus-sized particles (Fig. 7.8a). Simulations also indicate that there is an observable red-shift when nanoparticles 20–100 nm in diameter are captured *only* at the defect, suggesting that 2D-PhCs are ideal for detecting virus-sized objects (Fig. 7.8b).

Almost all demonstrations of single particle sensitivities for 2D-PhCs use latex or polymeric spheres with refractive indices that are much higher than biological molecules (n = 1.45 vs. n = 1.35). It is well known that measured sensitivities are significantly higher when the refractive index contrast is large; therefore, it is important to use biological particles to demonstrate virus particle detection, which occurs with much less refractive index contrast. After showing that 2D-PhCs could be used to capture proteins and measure antibody/antigen interactions, the capability of the 2D-PhC devices to detect viruses was pursued. Using the same multiplexed transmission design previously described for h-IgG detection, detection experiments with ~55 nm diameter human papilloma virus-like particles (HP-VLP) were performed. HP-VLPs served as model viral pathogens, since they contained intact capsids but no replication machinery, and were therefore non-infectious and safe to handle. Motivated by the need to detect viruses at low concentrations from complex matrices (such as blood), detection experiments were conducted in 10 % bovine serum (Fig. 7.9a). It was found that the 2D PhC retained the ability to selectively and specifically detect HPV VLPs with no appreciable loss in signal (red-shift). Furthermore, mostly intact virus particles were captured, since using antibodies specific for intact capsids had significantly more red-shift compared to antibodies specific for the denatured form or with none at all (Fig. 7.9b). In addition to confirming that viruses could be captured selectively, the limit-of-detection was determined from an experimental dose-dependent response of HP-VLPs captured with multiple 2D-PhCs (Fig. 7.9c). Results demonstrated a detection limit in the low nanomolar range, similar to that observed with h-IgG,

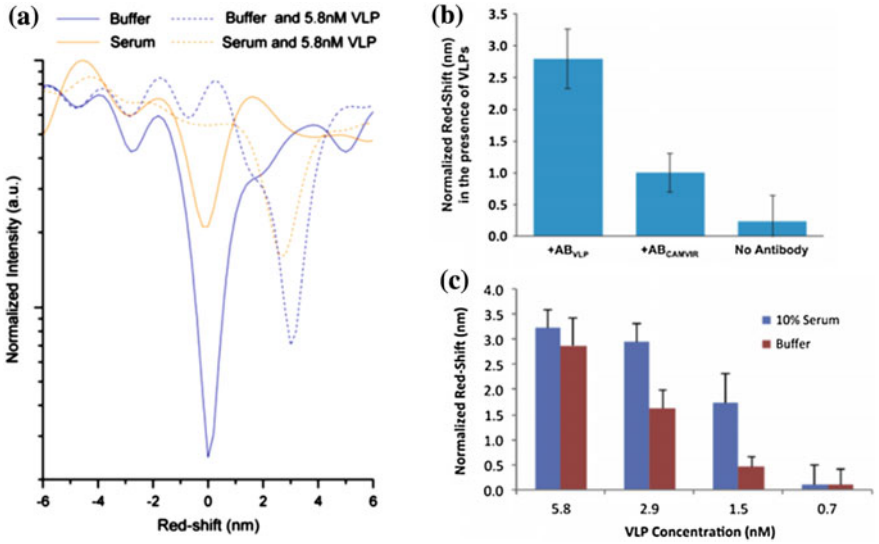

Fig. 7.9 Capture and quantitative detection of human papillomavirus-like particles (HP-VLP). Virus-like particles could be captured in buffer and 10 % serum with no noticeable difference in red-shift (**a**). Detection was sensitive for intact virus-like particles determined by using antibodies specific for the whole virus (**b**, $+AB_{VLP}$) compared to antibodies specific for denatured capsids (**b**, AB_{CAMVIR}) and absent any antibody (**c**, No Antibody)—error bars are standard deviations from average measurements (n=). Experimental dose-response of the 2D-PhC for different concentrations of HP-VLP in either 10 % serum or buffer (**c**)—error bars are the root-sum-squares of the standard deviation of red-shifts for the target and control chips

with a sensitivity of 0.5 nm/nM red-shift. These data provided the first demonstration that 2D-PhCs can serve as effective sensors for model viral pathogens, with high selectivity and low non-specific binding in serum [52].

7.5 Enhancing Sensitivity Through Directed Functionalization

Though detection was observed with 2D-PhCs, large amounts of target binding to areas outside the biosensor was expected to occur, since the functionalization procedure to capture biomolecules occurs not only at the crystal, but to the entire chip surface. It is well known that current methods of antibody immobilization, regardless of the type of label-free biosensor, can significantly deplete target (especially at low concentrations) and worsen the limit of detection [15, 19, 49]. While optical label-free biosensors have the capability to detect single particles (high sensitivity), in practice, this goal has been difficult to achieve. Capturing targets at low concentrations is fundamentally limited by the diffusion of molecules

and their binding to nanometer scale surfaces, which has been predicted to have picomolar detection limits within a reasonable time length for bioassays [50]. However, the reported detection limits for ultra-sensitive biosensors are significantly worse [14]. This is partly due to the placement of capture molecules over areas that are much larger than the sensor. In order to improve detection limits to match those of simulations, capture molecules need to be placed *only* on the active areas of nanoscale devices. However, this is nontrivial and an important issue that has not been specifically addressed in literature. Current immobilization strategies functionalize both sensing and non-sensing regions due to the inability to precisely place probes with nanometer precision in a reproducible and scalable way. As is often the case, large areas of surface are functionalized with probe molecules, and this in turn leads to target depletion and diminished limits of detection [49, 51, 52]. Since almost all optical label-free biosensors incorporate nanoscale features into their sensing modality, the topography of the design can potentially be exploited for selective functionalization of probe molecules. As discussed above, the Rochester group demonstrated that 2D-PhCs had nanomolar detection limits for proteins and viruses [38, 53]. Since the device was small (total area of 70 μm^2), it was hypothesized that the limit of detection could be improved if deposition of capture molecules was limited only to the photonic crystal. To test this hypothesis, a proof-of-concept experiment was performed, in which the ability of protein blocking nanoparticles (poly N-isopropylacrylamide, PNIPAM) to self-assemble around the distinct topography of a 2D PhC was exploited. Building on the previous work of Lyon, Serpe, and others that showed that PNIPAM nanoparticles readily self-assemble on surfaces [54, 55], we demonstrated that microgels self-assemble in a topographically selective manner—that is, they formed well packed patterns on planar surfaces, but did not enter into the well regions of the photonic crystal (Fig. 7.10).

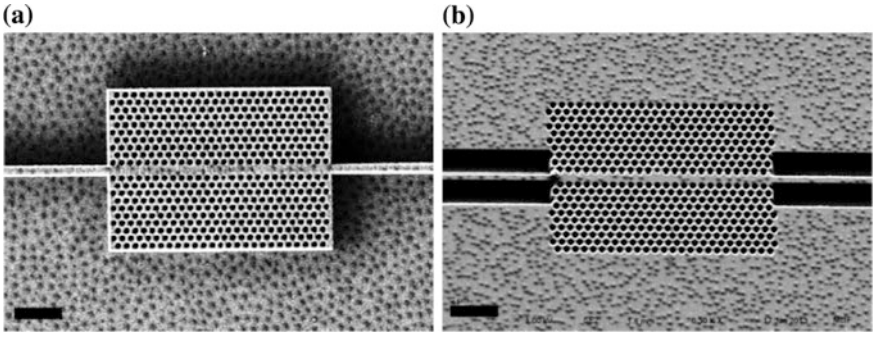

Fig. 7.10 Negative (**a**) and positive (**b**) 2D-PhC designs coated by dip-coating chips in a solution of protein blocking poly-N isopropylacrylamide micro-particles. Upon drying, particles spontaneously assembled into mosaic patterns in a topographically selective manner, avoiding the nanostructured regions of the photonic crystals

It was expected the large particle assemblies would block proteins from binding to the non-active surfaces and enhance the limit of detection by localizing capture molecules (antibody) to the photonic crystal but not the surrounding regions. Red-shifts of particle coated and control crystals were obtained for the IgG/h-IgG protein system. Red-shifts at 5.8 nM target were observed to be higher when antibody was localized to the photonic crystals compared to controls without nanoparticles (Fig. 7.11a). A dose-dependent response of IgG showed that immobilization of protein blocking nanoparticle onto the 2D-PhC surface caused the detection limit to improve by a factor of 100, closely matching the expected value from simulation (Fig. 7.11b, c) [56]. This method of blocking was simple, cost-effective, and could easily be modified to work for other types of label-free

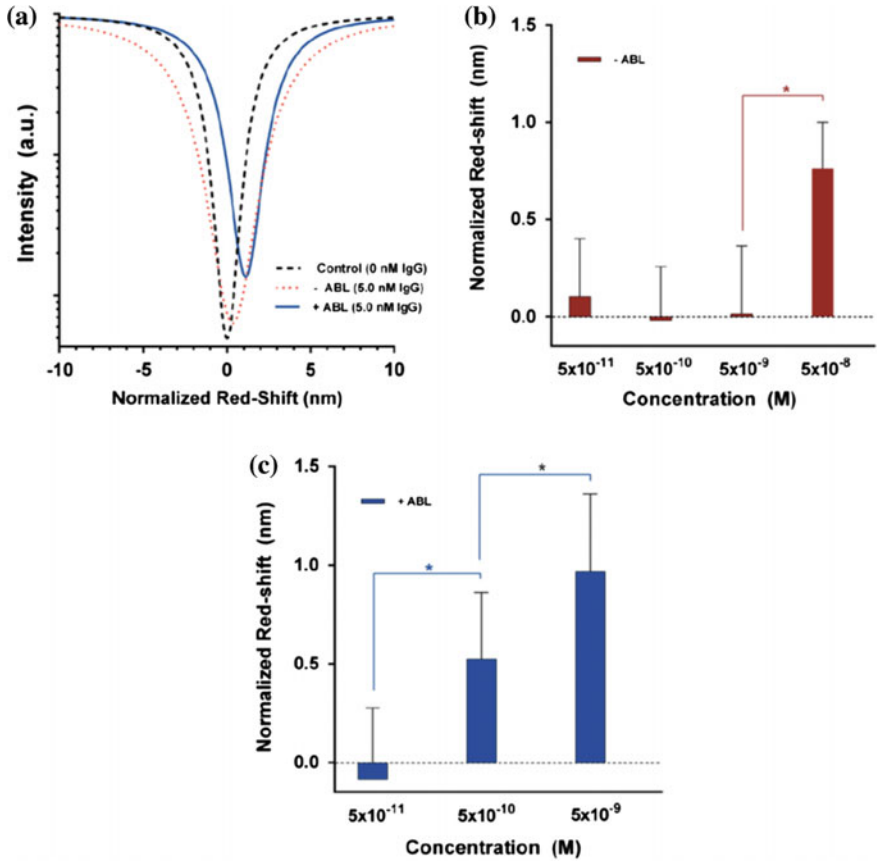

Fig. 7.11 2D-PhC capture of h-IgG with and without antibody localization (ABL) using protein blocking nanoparticles. At a high concentration, the red-shift was clearly observed (**a**). Without ABL, the highest observed concentration was 50 nM (**b**), while ABL the lower limit of detection was 0.5 nM (**c**). Error bars were calculated by taking the square root of the sum of the squares of the standard deviations between the experimental and control red-shifts

sensors. The key result of this work showed that simply adjusting the location of capture molecules to only the active regions of the device had large impacts on the lower limit of detection for 2D-PhCs.

One key problem with label-free sensing is the inability to discriminate between specific and non-specific binding of target molecules, which can severely restrict limits of detection and sensitivity. This is a particularly challenging problem with complex samples, such as serum, saliva, or other matrices that contain many molecules across a broad range of concentrations, all of which interfere with targeted detection. Recently, new crystal designs have been proposed which can monitor specific red-shifts resulting from target capture, while simultaneously and independently identifying non-specific binding. In most sensing experiments, a separate reference device (in this case a 2D-PhC) is treated in an identical manner to an experimental chip, except that the capture molecules are not immobilized. However, this method has several disadvantages. While the requirement that a portion of the total number of devices be dedicated as controls is most obvious, measurement of spectra either in parallel or in series means that performance deviations between devices as well as extrinsic factors, such as temperature or drift, are difficult to track. Sample composition can also change from experiment to experiment (especially with complex matrices), and so an on-chip and direct

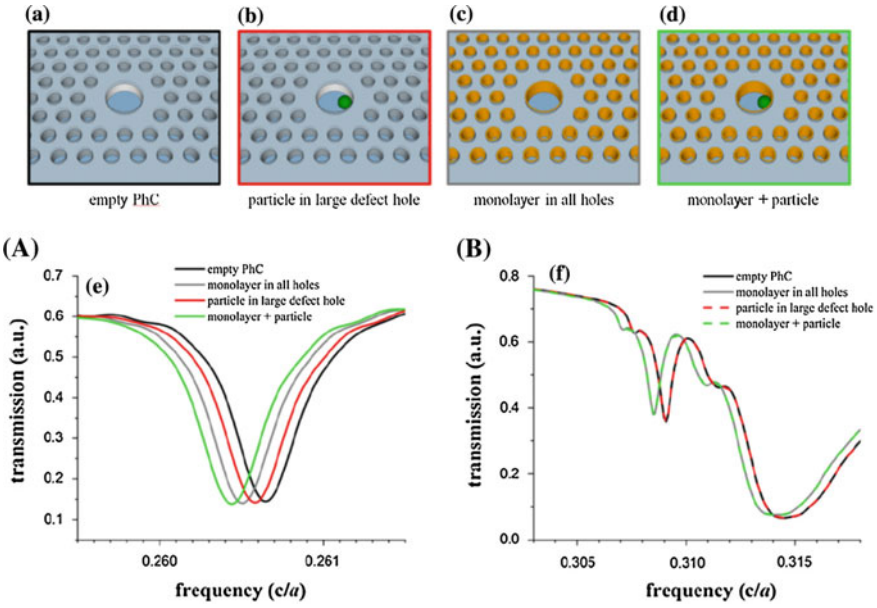

Fig. 7.12 Simulations of photonic crystals empty (*top*, **a**), containing a single large particle (*top*, **b**), coated with a monolayer of material (*top*, **c**), and with both particle and monolayer (*top*, **d**). Results show that the maximum absorption wavelength red-shifts when material is bound anywhere on the crystal (**A**), while the band-edge only shifts if material is present in the defect (**B**). Note, the x-axis is in units of frequency, and so a red-shift in wavelength is observed as a decrease in frequency

method is needed to monitor these types of changes on a sample-by-sample basis. A recent design from the Rochester group proposes a new way measure both specific and non-specific effects by monitoring the effects of band-edge shifting to determine if material is exclusively captured in the defect or by the surrounding neighboring wells (Fig. 7.12) [40]. The band-edge was found to be insensitive to monolayer thicknesses added to the 2D-PhC outer wells, but would shift if material were captured inside the defect. In this case, a large defect was fabricated so that selective capture of viruses and discrimination from particulates binding inside smaller, neighboring wells could be obtained.

7.6 Current Challenges and Future Outlook for 2D-PhCs

2D-PhCs serve as sensitive sensors for biodetection. In work conducted to date, experiments have demonstrated optical label-free detection of protein and viral targets in the presence of complex matrices. Additionally, unique designs may enable observation of changes at specific regions of the photonic crystals, enabling the discrimination between specific and non-specific binding based both on specific recognition and on the intrinsic geometry and optical properties of the crystal.

While these are encouraging results, the performance of 2D PhCs in "real world" applications remains far from the single-particle detection capability predicted by theory (and demonstrated for nonselective capture of latex particles in early experiments using highly specialized conditions). To close this gap, significant additional advances are required. First, as discussed in a seminal paper by Sheehan and Whitman [50], the sensitivity of nanoscale sensors is generally limited by the amount of material that can diffuse to the active area of the sensor within a "reasonable" time frame. Integration of the sensor with microfluidic channels can address the transport issue to an extent. However, further strategies will be needed to reach ultimate sensitivity. One promising approach is to utilize the optical trapping properties of the crystal to enhance binding; preliminary efforts along these lines have been published by our group and others [57–59]. Integration of sensors into full "lab on a chip" systems is also an important frontier: as stated at the outset, the dimensions and materials of 2D PhCs are compatible with standard photolithographic processes. Thus, when combined with an appropriate packaging strategy for on-chip light sources and detectors, reaching this goal should be feasible.

References

1. L. Clark, C. Lyons, Electrode systems for continuous monitoring in cardiovascular surgery. Ann. N. Y. Acad. Sci. **102**, 29–455 (1962)
2. A. McFarlane, Efficient trace-labelling of proteins with iodine. Nature **182**, 53 (1958)
3. R. Rice, G. Means, Radioactive labeling of proteins in vitro. J. Biol. Chem. **246**, 831–832 (1971)

4. A. Hershey, M. Chase, Independent functions of viral proteins and nucleic acid in growth of bacteriophage. J. Gen. Physiol. **36**, 39–56 (1952)
5. L.A. Sternberger, P.H. Hardy, J.J. Cuculis, H.G. Meyer, The unlabeled antibody enzyme method of immunohistochemistry: preparation and properties of soluble antigen-antibody complex (horseradish peroxidase-antihorseradish peroxidase) and its use in identification of spirochetes. J. Histochem. Cytochem. Cytochem. **18**, 315–333 (1970)
6. J.L. Cordell, B. Falini, W.N. Erber, A.K. Ghosh, Z. Abdulaziz, S. MacDonald, K.A. Pulford, H. Stein, D.Y. Mason, Immunoenzymatic labeling of monoclonal antibodies using immune complexes of alkaline phosphatase and monoclonal anti-alkaline phosphatase (APAAP complexes). J. Histochem. Cytochem. **32**, 219–229 (1984)
7. E. Engvall, P. Perlmann, Enzyme-linked immunosorbent assay, ELISA III. Quantitation of specific antibodies by enzyme-labeled anti-immunoglobulin in antigen-coated tubes. J. Immunol. **109**, 129–135 (1972)
8. T.H. The, T.E. Feltkamp, Conjugation of fluorescein isothiocyanate to antibodies. I. Experiments on the conditions of conjugation. Immunology **18**, 865–873 (1970)
9. D. Ivnitski, I. Abdel-Hamid, P. Atanasov, E. Wilkins, Biosensors for detection of pathogenic bacteria. Biosens. Bioelectron. **14**, 599–624 (1999)
10. K.K. Jain, Applications of nanobiotechnology in clinical diagnostics. Clin. Chem. **53**, 2002–2009 (2007)
11. J. Homola, S.S. Yee, G. Gauglitz, Surface plasmon resonance sensors: review. Sens. Actuators B Chem. **54**, 3–15 (1999)
12. J. Lu, C.M. Strohsahl, B.L. Miller, L.J. Rothberg, Reflective interferometric detection of label-free oligonucleotides. Anal. Chem. **76**, 4416–4420 (2004)
13. C.R. Mace, C.C. Striemer, B.L. Miller, Detection of human proteins using arrayed imaging reflectometry. Biosens. Bioelectron. **24**, 334–337 (2008)
14. X. Fan, I.M. White, S.I. Shopova, H. Zhu, J.D. Suter, Y. Sun, Sensitive optical biosensors for unlabeled targets: a review. Anal. Chim. Acta **620**, 8–26 (2008)
15. L.M. Bellan, D. Wu, R.S. Langer, Current trends in nanobiosensor technology. Wiley Interdiscip. Rev. Nanomed. Nanobiotechnol. **3**, 229–246 (2011)
16. L. Feuz, P. Jönsson, M.P. Jonsson, F. Höök, Improving the limit of detection of nanoscale sensors by directed binding to high-sensitivity areas. ACS Nano **4**, 2167–2177 (2010)
17. F. Patolsky, G. Zheng, O. Hayden, M. Lakadamyali, X. Zhuang, C.M. Lieber, Electrical detection of single viruses. Proc. Natl. Acad. Sci. USA **101**, 14017–14022 (2004)
18. H. Zhu, I.M. White, J.D. Suter, M. Zourob, X. Fan, Opto-fluidic micro-ring resonator for sensitive label-free viral detection. Analyst **133**, 356–360 (2008)
19. R.L. Caygill, G.E. Blair, Pa Millner, A review on viral biosensors to detect human pathogens. Anal. Chim. Acta **681**, 8–15 (2010)
20. S. Olivier, M. Rattier, H. Benisty, C. Weisbuch, C.J.M. Smith, R.M. De La Rue, T.F. Krauss, U. Oesterle, R. Houdré, Mini-stopbands of a one-dimensional system: the channel waveguide in a two-dimensional photonic crystal. Phys. Rev. B **63**, 113311 (2001)
21. J.D. Joannopoulos, Molding the flow of light. MIT Annual 32–43 (2001)
22. M.R. Lee, P.M. Fauchet, Two-dimensional silicon photonic crystal based biosensing platform for protein detection. Opt. Express **15**, 4530–4535 (2007)
23. A. Ulhir, Electrolytic shaping of germanium and silicon. Bell Syst. Tech. J. **35**, 333 (1956)
24. T.R. Turner, Electropolishing silicon in hydrofluoric acid solutions. J. Electrochem. Soc. **105**, 402–408 (1958)
25. L.T. Canham, Silicon quantum wire array fabrication by electrochemical and chemical dissolution of wafers. Appl. Phys. Lett. **57**, 1046–1048 (1990)
26. A. Janshoff, K.-P.S. Dancil, C. Steinem, D.P. Greiner, V.S.-Y. Lin, C. Gurtner, K. Motesharei, M.J. Sailor, M.R. Ghadiri, Macroporous p-type silicon Fabry-Perot layers. Fabrication, characterization, and applications in biosensing. J. Am. Chem. Soc. **120**, 12108–12116 (1998)
27. M.J. Sailor, Color me sensitive: amplification and discrimination in photonic silicon nanostructures. ACS Nano **1**, 248–251 (2007)

28. S. Chan, P.M. Fauchet, Y. Li, L.J. Rothberg, B.L. Miller, Porous silicon microcavities for biosensing applications. Phys. Status Solidi A **182**, 541–546 (2000)
29. R.D. Hubbard, S.R. Horner, B.L. Miller, Highly substituted *ter*-cyclopentanes as receptors for lipid A and simple carbohydrates in aqueous solution. J. Am. Chem. Soc. **123**, 5810–5811 (2001)
30. S. Chan, S.R. Horner, B.L. Miller, P.M. Fauchet, Identification of gram negative bacteria using nanoscale silicon microcavities. J. Am. Chem. Soc. **123**, 11797–11798 (2001)
31. H. Ouyang, M. Christophersen, R. Viard, B.L. Miller, P.M. Fauchet, Macroporous silicon microcavities for macromolecule detection. Adv. Func. Mat. **15**, 1851–1859 (2005)
32. L.M. Bonanno, T.C. Kwong, L.A. DeLouise, Label-free porous silicon immunosensor for broad detection of opiates in a blind clinical study and results comparison to commercial analytical chemistry techniques. Anal. Chem. **82**, 9711–9718 (2010)
33. L.A. DeLouise, P.M. Fauchet, B.L. Miller, A.P. Pentland, Hydrogel-supported optical microcavity sensors. Adv. Mater. **17**, 2199–2203 (2005)
34. C.-S. Huang, S. George, M. Lu, V. Chaudhery, R. Tan, R.C. Zangar, B.T. Cunningham, Application of photonic crystal enhanced fluorescence to cancer biomarker microarrays. Anal. Chem. **83**, 1425–1430 (2011)
35. B.T. Cunningham, Photnic crystal surfaces as a general purpose platform for label-free and fluorescent assays. J. Assoc. Lab. Automation **15**, 120–135 (2010)
36. L.L. Chan, M. Pineda, J.T. Heeres, P.J. Hergenrother, B.T. Cunningham, A general method for discovering inhibitors of protein-DNA interactions using photonic crystal biosensors. ACS Chem. Biol. **3**, 437–448 (2008)
37. S. Mandal, J.M. Goddard, D. Erickson, A multiplexed optofluidic biomolecular sensor for low mass detection. Lab Chip **9**, 2924–2932 (2009)
38. S. Pal, P.M. Fauchet, B.L. Miller, 1-D and 2-D photonic crystals as optical methods for amplifying biomolecular recognition. Anal. Chem. **84**, 8900–8908 (2012)
39. S. Pal, E. Guillermain, R. Sriram, B.L. Miller, P.M. Fauchet, Silicon photonic crystal nanocavity-coupled waveguides for error-corrected optical biosensing. Biosens. Bioelectron. **26**, 4024–4031 (2011)
40. M.R. Lee, P.M. Fauchet, Nanoscale microcavity sensor for single particle detection. Opt. Lett. **32**, 3284–3286 (2007)
41. J.E. Baker, B.L. Miller, Discrimination of specific and nonspecific binding in two-dimensional photonic crystals. Opt. Express **23**(6), 7101–7110 (2015)
42. S. Pal, E. Guillermain, R. Sriram, B.L. Miller, P.M. Fauchet, Microcavities in photonic crystal waveguides for biosensor applications. Proc. SPIE **7553**, 755304 (2011)
43. B.G. Brenner, M. Roger, J.P. Routy, D. Moisi, M. Ntemgwa, C. Matte, J.G. Baril, R. Thomas, D. Rouleau, J. Bruneau, R. Leblanc, M. Legault, C. Tremblay, H. Charest, M.A. Wainberg, Quebec primary HIV infection study group. High rates of forward transmission events after acute/early HIV-1 infection. J. Infect. Dis. **195**, 951–959 (2007)
44. M.C. Strain, S.M. Lada, T. Luong, S.E. Rought, S. Gianella, V.H. Terry, C.A. Spina, C.H. Woelk, D.D. Richman, Highly precise measurement of HIV DNA by droplet digital PCR. PLoS ONE **8**, e55943 (2013)
45. J. Zhang, J.P. Lang, F. Huber, A. Bietsch, W. Grange, U. Certa, R. Mckendry, H.-J. Güntherodt, M. Henger, Ch. Gerber, Rapid and label-free nanomechanical detection of biomarker transcripts in human RNA. Nat. Nanotechnol. **1**, 214–220 (2006)
46. R. Luo, M.J. Piovoso, R. Zurakowski, Modeling uncertainty in single-copy assays for HIV. J. Clin. Microbiol. **50**, 3381–3382 (2012)
47. H. Mukundan, A.S. Anderson, W.K. Grace, K.M. Grace, N. Hartman, J.S. Martinez, B.I. Swanson, Waveguide-based biosensors for pathogen detection. Sensors (Basel). **9**, 5783–5809 (2009)
48. H.K.P. Mulder, A. Ymeti, V. Subramaniam, J.S. Kanger, Size-selective detection in integrated optical interferometric biosensors. Opt. Express **20**, 20934–20950 (2012)
49. C.I.L. Justino, T.A. Rocha-Santos, A.C. Duarte, Review of analytical figures of merit of sensors and biosensors in clinical applications. Trends Anal. Chem. **29**, 1172–1183 (2010)

50. P.E. Sheehan, L.J. Whitman, Detection limits for nanoscale biosensors. Nano Lett. **5**, 803–807 (2005)
51. R.P. Ekins, Ligand assays: from electrophoresis to miniaturized microarrays. Clin. Chem. **44**, 2015–2030 (1998)
52. R.P. Ekins, F. Chu, Multianalyte microspot immunoassay–microanalytical "compact disk" of the future. Clin. Chem. **37**, 1955–1967 (1991)
53. S. Pal, A.R. Yadav, M.A. Lifson, J.E. Baker, P.M. Fauchet, B.L. Miller, Selective virus detection in complex sample matrices with photonic crystal optical cavities. Biosens. Bioelectron. **44**, 229–234 (2013)
54. M.J. Serpe, L.A. Lyon, Colloidal hydrogel microlenses. Adv. Mater. **16**, 184–187 (2004)
55. M.J. Serpe, C.D. Jones, L.A. Lyon, Layer-by-layer deposition of thermoresponsive microgel thin films. Langmuir **19**, 8759–8764 (2003)
56. M.A. Lifson, D.J. Basu Roy, B.L. Miller, Enhancing the detection limit of nanoscale biosensors via topographically selective functionalization. Anal. Chem. **86**, 1016–1022 (2014)
57. A.T. Heiniger, B.L. Miller, P.M. Fauchet, Proc. SPIE **7888**, 78880L (2011)
58. N. Descharmes, U.P. Dharanipathy, Z. Diao, M. Tonin, R. Houdré, Phys. Rev. Lett. **110**, 123601 (2013)
59. N. Descharmes, U.P. Dharanipathy, Z. Diao, M. Tonin, R. Houdré, Lab Chip **13**, 3268–3274 (2013)